Frequency Domain Approach for Dynamics Identification of the Actuator with Asymmetric Hysteresis*

Zhiyong Sun[1], Yu Cheng[2], Ning Xi[1] Sheng Bi[1], Congjian Li[1], Bo Song[2], Ruiguo Yang[3], Lina Hao[4], and Liangliang Chen[2]

***Abstract*— Micro/nano-manipulation systems have been developed and utilized for decades due to their irreplaceable roles in fields such as MEMS/NEMS fabrication and biological studies. Generally, the motion precision of a micro/nano-manipulator highly depends on its actuator, whose performance can be enhanced by proper control strategies. To design satisfactory controllers, an accurate plant model is ideal. For micro/nano-manipulators, the implemented actuators are mostly Smart Materials (SMs), which exhibit strong hysteretic and dynamic coupling characteristics. The construction of linear dynamics preceded by hysteresis is a prevalent representation for describing SM actuators' behaviors. To effectively and accurately model SM actuators, this paper employs the Extended Unparallel Prandtl-Ishlinskii (EUPI) model to describe complicated hysteretic behaviors. For modeling dynamics of SM actuators, firstly, the EUPI inverse is implemented to compensate the hysteretic effect of the plant; subsequently, the Weighted Complex Least-Squares (WCLS) identification method is proposed to estimate parameters of the dynamic part in the form of complex number function. To guarantee stability of the identified model, the Particle Swarm Optimization based WCLS (PSO-WCLS) optimization approach is proposed. The advantage of the proposed modeling scheme is that, it is capable of accurately describing complicated hysteresis of SM actuators and does not require the drive signal to be small while modeling its dynamics; besides this scheme contains frequency domain identification merits, such as easy noise reduction and easy combination of data from different experiments. The modeling and identification scheme is verified through comparison tests conducted on a piezoelectric actuator platform.**

I. INTRODUCTION

Micro/nano-manipulation systems such as Atomic Force Microscopy (AFM), Scanning Ion Conductance Microscopy (SICM) have been widely implemented and playing irreplaceable roles in fields of MEMS/NEMS fabrication, ultra-high precision manufacturing and biological studies [1], [2]. The motion precision of a micro/nano manipulation system highly depends on the implemented actuator, which consists mostly of Smart Materials (SMs) for advantages of high spatial resolution, fast response, flexible structure and easy manufacturing properties [3]–[5]. Most SMs exhibit hysteresis, dynamics coupling characteristics. To date, two prevalent SM actuator modeling approaches, hysteresis/dynamics parallel model [6], [7] and cascade model [8]–[12] have been widely employed in advanced controllers design. The parallel model has an additive relation between its hysteretic and dynamic portions, which is relatively easy to estimate the associated parameters. However, the parallel model is not suitable for capturing high frequency behaviors, and its dynamic portion is typically used for describing relatively slow behaviors [7], [13].

The cascade model possesses hysteretic and dynamic cascade construction, which is more suitable for describing SM actuators with high frequency response. The cascade model is prevalently represented as linear dynamics preceded by hysteresis construction (as shown in Fig. 1), where the dynamic portion is commonly built as a transfer function for easy frequency and uncertainty analysis [8]. The hysteretic behavior is more complicated, since it is intrinsically nonlinear. To represent hysteretic phenomena accurately, lots of practical modeling approaches have been reported, such as operator based superposition models including the Preisach model [7], Prandtl-Ishlinskii (PI) model [6], and the Generalized PI (GPI) operator based model [14]. Bouc-Wen hysteresis model is in the category employing differential equations representation [9].

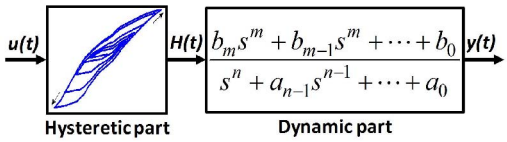

Fig. 1. Linear dynamics preceded by hysteresis model of SM actuators.

Prisach operator can effectively describe most static hysteresis phenomena [15], [16], however it is not very efficient since it requires to employ a great amount of operators to meet satisfactory precision [17]. As an alternative, PI model was developed and have been widely adopted for its convenient description and analytical inverse representation [6], [18]. However, the symmetric property of the Classical PI (CPI) operator hinders its further application in complicated hysteresis modeling [14]. Similar as the PI model, the differential equation based Bouc-Wen model has fewer tunable parameters, which limits its performance on

*This work was supported in part by the U. S. Army Research Laboratory and the U. S. Army Research Office under the Grant W911NF-16-1-0572.

[1]Z. Sun, S. Bi, C. Li and N. Xi are with Department of Industrial and Manufacturing Systems Engineering, The University of Hong Kong, Pokfulam, Hong Kong SAR {sunzy, shengbi, congjian.li, xining}@hku.hk

[2]Y. Cheng, B. Song and L. Chen are with Department of Electrical and Computer Engineering, Michigan State University, East Lansing, MI, 48824, USA {chengyu9, songbo, chenlia5}@msu.edu

[3]R. Yang is with Department of Mechanical and Materials Engineering, University of Nebraska-Lincoln, Lincoln, NE, 68588 USA ryang6@unl.edu

[4]L. Hao is with School of Mechanical Engineering and Automation, Northeastern University, Shenyang, Liaoning, 110819, China haolina@me.neu.edu.cn

modeling complicated hysteresis. To date, great efforts have been focused on complicated hysteresis modeling, such as a memoryless function was added to the CPI model to generate saturation property [19] and a memoryless function was used to re-map output of CPI model to generate asymmetric property [20]; literature [14] proposes to use generalized envelop functions to describe complicated hysteresis loops. However, challenge still exists. The memoryless function modified PI model cannot represent hysteresis flexibly, since their ascending/descending branches share same parameters; while the GPI model is hard to design, mostly because selection of the invertible envelop functions is empirical.

To accurately model SM actuators with linear dynamics-hysteresis cascade input-output relation, in this study, the Extended Unparallel PI (EUPI) model is employed to capture the hysteretic behavior considering its simplicity and capability of accurately describing complicated hysteresis [21]. To model dynamics of SM actuators, firstly the hysteresis inverse is designed and implemented to reduce the hysteretic effect [13]; subsequently, the weighted complex least-squares (WCLS) identification method is derived to estimate frequency domain dynamics represented as a complex number function. To guarantee stability of the identified model, the Particle Swarm Optimization based WCLS (PSO-WCLS) identification method is employed. Basically, this algorithm searches optimal parameters under stability constraints. The advantages of this entire modeling and identification scheme are: it can describe complicated hysteresis with high precision; it does not require the drive signal to be small while identifying SM actuator's dynamics; it contains the frequency domain identification merits, such as easy noise reduction and easy combination of data from different experiments [22], [23]. To verify the proposed modeling and identification scheme, the piezoelectric actuator, which is mostly employed in micro/nano-manipulation systems [1], [9], is modeled and identified. Comparison tests were conducted, where the MATLAB graphic identification toolbox was employed as the benchmark.

The remaining contents are arranged as following: in section II, the EUPI hysteresis modeling approach is briefly reviewed and the stable compensator design technique is addressed; in section III, the WCLS identification method is derived and the PSO-WCLS stable model identification algorithm is presented; in section IV, a piezoelectric actuator platform is set up to verify the proposed identification scheme; section V concludes this study.

II. REVIEW OF THE EUPI HYSTERESIS MODELING AND COMPENSATION APPROACH

A. Hysteresis Modeling using EUPI Model

In this study, the EUPI model is utilized to capture complex hysteretic characteristic of SM actuators [21]. The basic UPI operator is defined as (1),

$$\begin{aligned} &F_{r_i,\alpha_j}[u](t) \\ &\quad = \max(u(t)-r_i,\ \min(\alpha_j(u(t)+r_i), F_{r_i,\alpha_j}(t^-))) \\ &\quad \text{with } t^- = \lim_{\delta\to 0^+}(t-\delta) \text{ and } r_i \geq 0,\ \alpha_j > 0, \end{aligned} \tag{1}$$

where $u(t)$ represents the drive signal at moment t, and r_i denotes the i^{th} threshold and the descending edge is tilted by multiplying a factor α_j. In particular, by setting the tilt parameter α_j to 1, the UPI operator becomes the CPI operator.

Typically, a complicated hysteresis can be decomposed into two parts: memory and memoryless components. Furthermore, the memory component can be separated into the symmetric and asymmetric parts. To facilitate compensator design and analysis, the EUPI model is built using the three components described as (2) [21],

$$\begin{cases} H[u](k) = \Gamma_{CPI}[u](k) + \Gamma_{UPI}[u](k) + P[u](k) \\ \Gamma_{CPI}[u](k) = a_0 u(k) + \sum_{i=1}^{N_h} b_i F_{r_i,1}[u](k) \\ \Gamma_{UPI}[u](k) = \sum_{i=1}^{N_r}\sum_{j=1}^{N_a} d_{ij} F_{r_i,\alpha_j}[u](k) \\ P[u](k) = \sum_{i=2}^{N_p} p_i u^i(k) + p_0 \\ \quad s.t.\ a_0,\ \alpha_j > 0,\ b_i,\ d_{ij},\ r_i \geq 0, \end{cases} \tag{2}$$

where $H[u](k)$ is the output of the EUPI model; $\Gamma_{CPI}[u](k)$, $\Gamma_{UPI}[u](k)$, and $P[u](k)$ are the CPI, UPI and polynomial parts, respectively; a_0 is a linear coefficient, which can be directly extracted to design controllers [12]; notation b_i, d_{ij} and p_i are the weight gains for the corresponding CPI operators, UPI and polynomial parts, respectively; N_h and N_p are the number of operators consisting the CPI and polynomial portion; N_a and N_r are the total levels for the tilt α_j and the threshold r_i in the UPI component; p_0 is an output offset associated with the hysteresis initial condition.

B. EUPI Model based Stable Compensator

Hysteresis compensator is efficient and practical for reducing hysteretic effect in open-loop systems. In order to compensate hysteretic influence efficiently, the built model should be utilized effectively [24]. As addressed in [13], without an analytical expression, the EUPI model based inverse is constructed in an indirect way. Based on construction of the EUPI model shown in (2), the CPI portion can be extracted to perform direct inverse action, and other portion should be formatted to link the inverse CPI portion (as shown in Fig. 2). Similar as the scheme proposed in [6], an iterative construction represented in (3) is adopted as the EUPI inverse.

$$\begin{aligned} u(k) &= H^{-1}[y_r](k) \\ &= \Gamma_{CPI}^{-1}(y_r(k) - \Gamma_{UPI}[u](k-1) - P[u](k-1)), \end{aligned} \tag{3}$$

where $\Gamma_{CPI}^{-1}[u](k)$ denotes the inverse of the CPI component, which can be directly calculated according to procedure in [6], and $y_r(k)$ represents the input reference signal.

It is noted that the inverse scheme shown in Fig. 2 possesses a closed-loop construction inside, indicating it requires to perform iteratively to approach the desirable solution. However, whether this procedure can converge is not obvious. As addressed in [13], the sufficient condition for designing a stable EUPI inverse scheme is described as

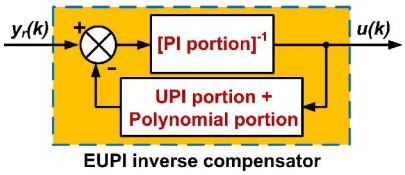

Fig. 2. Schematic diagram of the EUPI compensator.

(4) based on the well known small gain theorem.

$$a_0 > \max\left(\left|\frac{d(\Gamma_{UPI}[u](k)+P[u](k))}{du}\right|\right), \tag{4}$$

where a_0 denotes the linear coefficient of the CPI component in (2); $\Gamma_{UPI}[u](k)$ and $P[u](k)$ are the UPI and polynomial components, respectively.

It is noted that not all the directly built EUPI model can be utilized to construct the inverse scheme (3), since parameter a_0 may not be larger than the maximum gain of the rest part. It is also noted that, if a_0 is significantly larger than the possible gain of the rest part, the inverse scheme will converge much faster. Therefore, to guarantee the global stability of the compensator, one should manipulate the CPI and the rest component to significantly increase a_0 and reduce the maximum gain of the rest part. The adjustment can be conducted using (5), where a proportional gain k_{ex} is adopted to guarantee the stable condition described in (4).

$$\begin{aligned} H[u](k) = &(\Gamma_{CPI}[u](k)+k_{ex}u(k)) \\ &+(\Gamma_{UPI}[u](k)+P[u](k)-k_{ex}u(k)). \end{aligned} \tag{5}$$

Once condition (4) is satisfied, the function of the EUPI compensator will be a contract map [6]. According to the fix point theory, there exists a unique solution for any given $y_r(k)$.

III. DYNAMICS MODELING AND PSO-WCLS IDENTIFICATION APPROACH

A. Dynamics Modeling in Frequency Domain

Dynamic portion of a SM actuator is critical in controllers design, since it provides frequency dependent properties which influence the system stability seriously. Linear dynamic systems can be represented as Laplace domain format $D_p(s)$ in (6), which facilitates the frequency and uncertainty analysis,

$$D_p(s) = \frac{y(s)}{v(s)} = \frac{k_0(s^m+\cdots+g_j s^j+\cdots+g_0)}{s^n+\cdots+a_i s^i+\cdots+a_1 s+a_0}+D, \tag{6}$$

where $v(s)$ stands for the input of dynamic component $D_p(s)$, and the output of the hysteretic portion, as well; m is the numerator order, and it is strictly less than the denominator order n; D denotes the feedforward gain of the system, and k_0, a_i, g_j are associated parameters.

A transfer function can always be represented as a complex number function by replacing the Laplace variable s with a complex number ωj as shown in (7),

$$\begin{aligned} D_p(\omega j) &= \frac{b_n(\omega j)^n+b_{n-1}(\omega j)^{n-1}+\cdots+b_1(\omega j)+b_0}{(\omega j)^n+a_{n-1}(\omega j)^{n-1}+\cdots+a_1(\omega j)+a_0} \\ &= Re(\omega)+Im(\omega)j = A(\omega)e^{\alpha(\omega)}, \end{aligned} \tag{7}$$

where ω is the input frequency with unit rad/s; $A(\omega)$ and $\alpha(\omega)$ denote the magnitude and phase at frequency ω, respectively; $Re(\omega)$ and $Im(\omega)$ represent the real and imaginary parts of the transfer function regarding ω, respectively.

B. WCLS Identification Approach

Based on the complex number representation of (7), the parameters $[b_n, b_{n-1}, \cdots, b_0, a_n, \cdots, a_0]$ of a transfer function should be easily estimated using a Complex Least-Squares (CLS) identification approach. With this motivation, the CLS method is derived. To emphasize some essential data (features), the weighting method is introduced, as a combination, the estimation approach is called Weighted CLS (WCLS) identification method. To derive the WCLS approach, first, the objective function J is defined as:

$$\begin{aligned} &J = \textstyle\sum_{i=1}^{n} w_i(y_i-\hat{y}_i)\overline{(y_i-\hat{y}_i)} \\ \Rightarrow &J = (Y-\hat{Y})^T W\overline{(Y-\hat{Y})} \\ \Rightarrow &J = (Y-X^T\hat{\Theta})^T W\overline{(Y-X^T\hat{\Theta})}, \end{aligned} \tag{8}$$

where $X \in C^{n\times p}$ denotes the regression variable in the complex domain; $Y = [y_1, y_2, \cdots, y_n]^T \in C^{n\times 1}$ is the given data in the complex domain; $\hat{Y} = [\hat{y}_1, \hat{y}_2, \cdots, \hat{y}_n]^T \in C^{n\times 1}$ is the model output; $\hat{\Theta} \in R^{p\times 1}$ represents the real number parameters that need to be identified; $W \in \{\Lambda | \Lambda = \text{diag}(w_1, \cdots, w_n) \geq 0, w_i \in R\}$ is the weighting matrix to emphasize the interesting data, and $\overline{(\cdot)}$ represents the conjugate of the complex $(\cdot)$.

Via expanding X as $[x_{11}, \cdots, x_{1n}; \cdots; x_{n1}, \cdots, x_{nn}]$, objective function J can be represented as:

$$\begin{aligned} &J = \textstyle\sum_{i=1}^{n} w_i(y_i-\sum_{d=1}^{p}\theta_d x_{id})(\bar{y}_i-\sum_{d=1}^{p}\theta_d\bar{x}_{id}) \\ \Rightarrow &J = \textstyle\sum_{i=1}^{n} w_i[y_i\bar{y}_i-\sum_{d=1}^{p}\theta_d(\bar{x}_{id}y_i+x_{id}\bar{y}_i) \\ &\qquad +(\textstyle\sum_{d=1}^{p}\theta_d x_{id})(\sum_{d=1}^{p}\theta_d\bar{x}_{id})], \end{aligned} \tag{9}$$

where θ_d is the d^{th} parameter in $\hat{\Theta}$. Based on (9), J is then differentiated associated with θ_z, and is set to zero (as shown in (10)) to calculate the optimal θ_z.

$$\begin{aligned} \frac{\partial J}{\partial \theta_z} = &\textstyle\sum_{i=1}^{n} w_i[-(\bar{x}_{iz}y_i+x_{iz}\bar{y}_i) \\ &+(\textstyle\sum_{d=1}^{p}\theta_d\bar{x}_{id}x_{iz})+(\sum_{d=1}^{p}\theta_d x_{id}\bar{x}_{iz})] = 0. \end{aligned} \tag{10}$$

By rewriting (10), the following relation can be obtained:

$$\begin{aligned} &\textstyle\sum_{i=1}^{n} w_i(\bar{x}_{iz}y_i+x_{iz}\bar{y}_i) \\ =&\textstyle\sum_{i=1}^{n} w_i[(\sum_{d=1}^{p}\theta_d\bar{x}_{id}x_{iz})+(\sum_{d=1}^{p}\theta_d x_{id}\bar{x}_{iz})] \\ =&(\textstyle\sum_{d=1}^{p}\theta_d\sum_{i=1}^{n} w_i\bar{x}_{id}x_{iz})+(\sum_{d=1}^{p}\theta_d\sum_{i=1}^{n} w_i x_{id}\bar{x}_{iz}) \\ =&\textstyle\sum_{d=1}^{p}\theta_d(\sum_{i=1}^{n} w_i\bar{x}_{id}x_{iz}+\sum_{i=1}^{n} w_i x_{id}\bar{x}_{iz}). \end{aligned} \tag{11}$$

Consequently, by grouping associated variables together in (11), the following compact representation can be finally achieved,

$$\begin{aligned}&\left(X^T W\bar{X}+\bar{X}^T WX\right)\hat{\Theta}=\left(\bar{X}^T WY+X^T W\bar{Y}\right)\Rightarrow\\&\hat{\Theta}=\left(X^T W\bar{X}+\bar{X}^T WX\right)^{-1}\left(\bar{X}^T WY+X^T W\bar{Y}\right).\end{aligned}\tag{12}$$

The identified parameters in $\bar{\Theta}$ are always real since $\bar{X}^T WX$ is the conjugate of $X^T W\bar{X}$, so is the relation between $\bar{X}^T WY$ and $X^T W\bar{Y}$.

To apply the WCLS identification method in transfer function (7), it is required to format (7) as the following linear representation with unknown parameters at each frequency ω_i:

$$\begin{aligned}&Y(\omega_i j)=X(\omega_i j)Ae^{\alpha(\omega_i)}\\&\Rightarrow b_{\mathrm{n}}(\omega_i j)^n+b_{n-1}(\omega_i j)^{n-1}+\cdots+b_1(\omega_i j)+b_0\\&=A(\omega_i)e^{\alpha(\omega_i)}[(\omega_i j)^n+a_{n-1}(\omega_i j)^{n-1}+\cdots+a_0]\\&\Rightarrow\ X_i\cdot\hat{\Theta}=Y_i,\end{aligned}\tag{13}$$

where $\hat{\Theta}$, X_i and Y_i have the following expression:

$$\begin{aligned}&\hat{\Theta}=[\,b_{\mathrm{n}},b_{n-1},\cdots,b_1,b_0,a_{n-1},a_{n-2},\cdots,a_1,a_0\,]^T\\&X_i=[\,(\omega_i j)^{\mathrm{n}},(\omega_i j)^{n-1},\cdots,1,-A(\omega_i)e^{j\alpha(\omega_i)}(\omega_i j)^{n-1},\\&\qquad -Ae^{j\alpha(\omega_i)}(\omega_i j)^{n-2},\cdots,-A(\omega_i)e^{j\alpha(\omega_i)}\,]\\&Y_i=A(\omega_i)e^{j\alpha(\omega_i)}(\omega_i j)^n.\end{aligned}\tag{14}$$

Once (13) is achieved, the parameters of a transfer function can be simply calculated using (12).

C. PSO-WCLS Identification Approach for Stable Systems

The WCLS approach can optimize parameters for a transfer function regarding objective function $J(\hat{\Theta})$, however, it cannot guarantee the stability due to the influence of possible noise and nonlinear property of a plant. Usually, the stability constraint is complicated and may not be convex. To achieve stable representation for a system, a practical constrained identification approach is the Particle Swarm Optimization (PSO) method which can perform large scale searching with both directional and random properties.

In this paper, the PSO method is employed to search a suboptimal stable solution for modeling a plant. Basically, the denominator parameters are compacted into $P_{g,s}=[a_{n-1},\cdots,a_1,a_0]^T$, which is a particle in the PSO algorithm with s denoting the particle ID in one swarm, and g denoting the generation ID of that swarm. Once a particle $P_{g,s}$ is selected, (13) will be calculated with (15) to optimize the numerator parameters in $\hat{\Theta}_n=[b_n,b_{n-1},\cdots,b_0]^T$.

$$\begin{aligned}&X_i=[(\omega_i j)^n,(\omega_i j)^{n-1},\cdots,(\omega_i j),1]\\&X=[X_1^T,X_2^T,\cdots,X_n^T]^T\\&Y_i=A(\omega_i)e^{j\alpha(\omega_i)}\{(\omega_i j)^n+[(\omega_i j)^{n-1},\cdots,(\omega_i j),1]P_{g,s}\}\\&Y=[Y_1,Y_2,\cdots,Y_n]^T.\end{aligned}\tag{15}$$

After $P_{s,g}$ and $\hat{\Theta}_n$ are settled, the following fitness function T_e will be calculated considering the stability constraint. Once the stability constraint cannot be satisfied, the current particle will be discarded.

$$\begin{aligned}&T_e=\frac{1}{n}\sum_{i=1}^{n}\left|\frac{X_i\hat{\Theta}_n}{Y_i}-A(\omega_i)e^{(\alpha\omega_i)}\right|\\&s.t.\ \{P_{g,s}\,|\,Re(root(s^n+[s^{n-1},\cdots,1]P_{g,s}))<0\}.\end{aligned}\tag{16}$$

During identification, the frequency domain data will be first estimated using the WCLS method, subsequently the poles of the identified transfer function will be calculated. If some pole is outside the left half complex plane, the PSO stabilizing procedure will be triggered. The whole identification procedure can be addressed as following:

i) Format given frequency data into (14), and then run (12) to estimate the $\hat{\Theta}$. If the poles of the identified system are all on the left half complex plain, then go to step ***vi)***.

ii) The poles with positive part is flipped along the imaginary axis. The identified denominator parameters $[a_{n-1},\cdots,a_1,a_0]$ is calculated again using the stable poles, then the new parameters $[a'_{n-1},\cdots,a'_1,a'_0]$ are obtained.

iii) Around each parameter a'_i, a searching range will be defined, and particle entries are randomly scattered into these searching ranges. Subsequently, the fitness function (16) is calculated for each particle of the current swarm. After that, the particle with the minimum T_e will be assigned to $P_{g,opt}$ as the local optimal particle, which will be used to estimate the updating velocity of each particle.

iv) If the condition $T_e\le T_e^*$ is satisfied (T_e^* represents the selected error tolerance), the optimization algorithm will go to step ***vi)***.

v) The current optimal particle $P_{opt}\in\{P_{1,opt},P_{2,opt},\cdots,P_{g,opt}\}$ is the globally optimal particle with minimum T_e. The new generation swarm of particles is calculated as following:

$$\begin{cases}M=M_{max}-g\cdot\dfrac{M_{max}-M_{min}}{g_{max}},\\V_{g+1}=M\cdot V_g+c_1\cdot R_1\cdot(P_{g,opt}-P_{g,s})\\\qquad\qquad +c_2\cdot R_2\cdot(P_{opt}-P_{g,s}),\\P_{g+1,s}=P_{g,s}+V_{g+1},\end{cases}\tag{17}$$

where g denotes the generation of current swarm; V_g is the updating velocity; M is the inertial gain for generating smoother V_g, and M_{max}, M_{min} are the allowable maximum and minimum gains, respectively; c_1, c_2 are the weighting gains for emphasizing the local optimal direction and global optimal direction, respectively; R_1 and R_2 are positive definite random diagonal matrices for generating versatile particles. If the maximum generation g_{max} is not reached, then go back to step ***ii)***.

vi) Stop identification, calculate the optimal T_e, show the optimal particle and plot the T_e of each $P_{g,opt}$ along generations if applicable.

Remark 1: The reason for flipping the unstable poles along the imaginary axis in step ***ii)*** is that, this operation will not alter the optimal magnitude response of the identified transfer function, making use of it will reduce the swarm size, and benefit the particle searching procedure.

IV. EXPERIMENTAL SETUP AND PIEZOELECTRIC ACTUATOR MODELING VERIFICATION

An experimental platform for a piezoelectric actuator modeling test was set up. The platform as shown in Fig. 3(a) consists of a piezoelectric stack actuator (maximum output $21.3\mu m$ with maximum input $150V$), a custom-made one-dimensional fixed mechanism, one power amplifier (Amplification is 30), one capacitive sensor (effective resolution $20nm$), NI DAQ card (16-bit PCI-6221), and one computer with MATLAB and the real-time module installed. The EUPI compensator outputs signal to the power amplifier and collects actuator displacement data from the capacitive sensor via the DAQ card. The amplified compensation signal was directly applied to drive the piezoelectric actuator. The sampling rate for static hysteresis modeling was set to $0.1kHz$ because this procedure requires to capture very low-frequency (quasi-static) data, relatively low sampling frequency will reduce data amount. While modeling the dynamic part, the sampling rate was set to $10kHz$ to accurate capture the high frequency data.

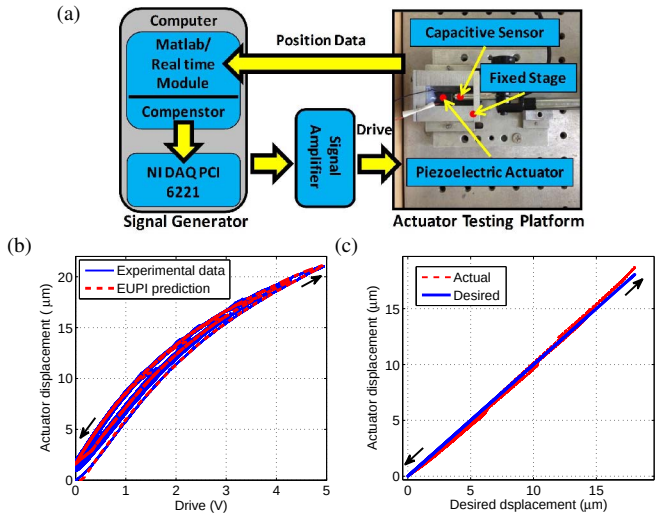

Fig. 3. Experimental setup, (a) piezoelectric actuator platform, (b) hysteresis raw data and model prediction data in the input-output domain, (c) hysteresis reduction using the designed EUPI compensator.

During building a hysteresis-linear-dynamics model, a quasi-static voltage signal was applied to drive the piezoelectric actuator for exciting the static hysteresis information. The collected data are shown in Fig. 3(b), which is asymmetric. By utilizing the EUPI model to represent the hysteresis phenomenon, the identification result is plotted with dotted curve. Based on the hysteresis portion model, the corresponding EUPI compensator was designed using the approach introduced in section II. The hysteresis compensation result is shown in Fig. 3(c), in which the hysteretic effect is greatly reduced in contrast to original data shown in Fig. 3(b).

To accurately model the dynamic portion of the actuator, the designed EUPI compensator was implemented to generate the drive signal to excite the actuator. The identification platform is shown in Fig.4, where the EUPI inverse processed chirp signal was applied to excite the piezoelectric actuator with selected frequency range. In this procedure, the input frequency was set to $0.01-50Hz$, since the integrated actuator system shows strong damping effect.

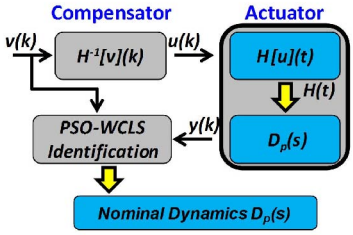

Fig. 4. Dynamics identification platform of the piezoelectric actuator.

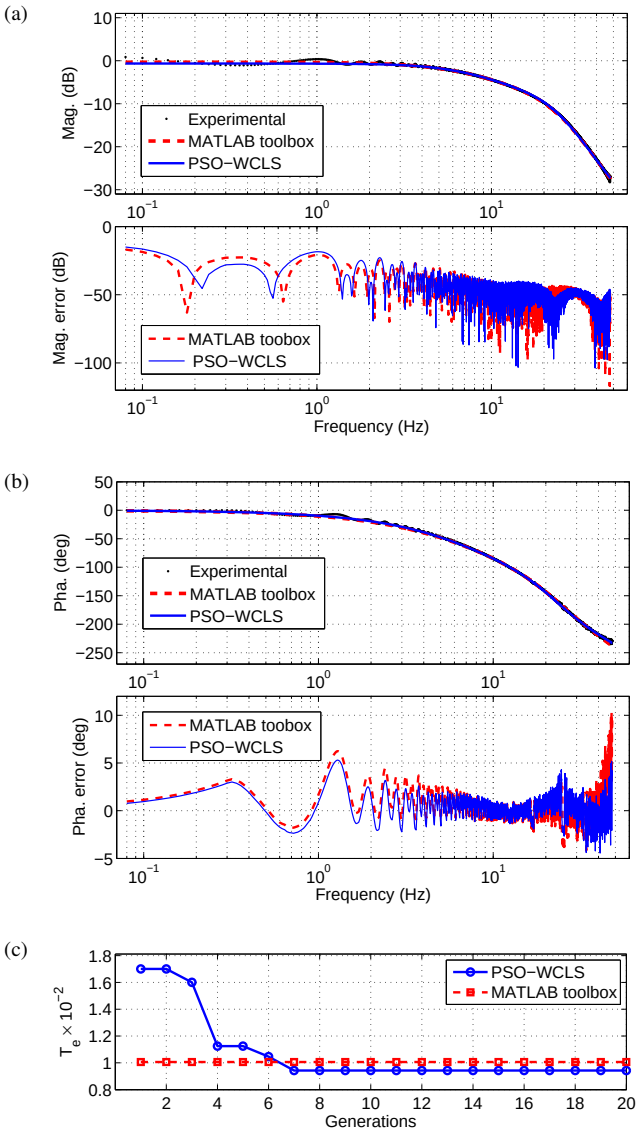

Fig. 5. Dynamics identification of the piezoelectric actuator, (a) magnitude response, modeling results and errors, (b) phase response, modeling results and errors, (c) T_es comparison along generations.

The actuator dynamics was identified using the PSO-WCLS approach with swarm size 100, maximum generation 20 and searching range $a_i' \cdot (1 \pm 0.5)$. The optimal T_e for each

generation is plotted in Fig. 5(c), where one can see the T_e becomes constant after 7 generations, since the objective $T_e^* \leq 0.01$ has been reached. The dynamics identification results are shown in Fig. 5(a), (b), which describe the plant magnitude and phase responses and the associated errors in the frequency domain using a 4^{th} order model with $[b_4, \cdots, b_0]$=[0.008933, -1.839, 260.4, 9.313×10^5, 3.096×10^7], and $[a_4, \cdots, a_0]$=[1, 244.2, 3.605×10^4, 1.898×10^6, 3.343×10^7]. It is noted that the magnitude response of the system decays seriously as input frequency increases. As benchmark, the transfer function estimation method of MATLAB graphic identification toolbox was employed, and the identified result is plotted in Fig. 5(a), (b), respectively. From the identification errors, one can see the proposed PSO-WCLS method and MATLAB identification approach have very close performances, however the proposed method shows better precision with smaller optimal T_e value illustrated in plot (c). The poles of the identified system are $100 \times [-0.8456 \pm 1.2107j, \ -0.3756 \pm 0.1105j]$, indicating it is stable.

V. CONCLUSIONS

In this study, the model of linear dynamics preceded by complicated hysteresis is employed to characterize behaviors of SM actuators. To precisely describe the hysteretic characteristic, the EUPI model is employed, which can describe hysteresis flexibly. To reduce the hysteretic influence during the dynamics identification, the stable EUPI inverse is established. The hysteresis inverse processed input-output dynamics data are utilized to directly identify the model parameters via the proposed WCLS approach. To guarantee stability of the identified model, the PSO-WCLS identification approach is proposed, which searches satisfactory parameters in a constrained non-convex space. The proposed identification scheme is verified with experiment on a piezoelectric actuator platform. As the benchmark, the MATLAB graphic identification toolbox is applied to estimate the dynamic component. The identification result shows that the proposed method achieves a better result compared to that obtained by the MATLAB toolbox.

REFERENCES

[1] R. Yang, B. Song, Z. Sun, K. W. C. Lai, C. K. M. Fung, K. C. Patterson, K. Seiffert-Sinha, A. A. Sinha, and N. Xi, "Cellular level robotic surgery: Nanodissection of intermediate filaments in live keratinocytes," *Nanomedicine: Nanotechnology, Biology and Medicine*, 2014.

[2] P. Li, L. Liu, Y. Wang, Y. Yang, C. Zhang, and G. Li, "Phase modulation mode of scanning ion conductance microscopy," *Applied Physics Letters*, vol. 105, no. 5, p. 053113, 2014.

[3] A. J. Fleming, "Nanopositioning system with force feedback for high-performance tracking and vibration control," *Mechatronics, IEEE/ASME Transactions on*, vol. 15, no. 3, pp. 433–447, 2010.

[4] H. Habibullah, H. R. Pota, I. R. Petersen, and M. Rana, "Tracking of triangular reference signals using lqg controllers for lateral positioning of an afm scanner stage," *Mechatronics, IEEE/ASME Transactions on*, vol. 19, no. 4, pp. 1105–1114, 2014.

[5] L. DeVries, F. D. Lagor, H. Lei, X. Tan, and D. A. Paley, "Distributed flow estimation and closed-loop control of an underwater vehicle with a multi-modal artificial lateral line," *Bioinspiration & biomimetics*, vol. 10, no. 2, p. 025002, 2015.

[6] P. Krejci and K. Kuhnen, "Inverse control of systems with hysteresis and creep," *IEE Proceedings-Control Theory and Applications*, vol. 148, no. 3, pp. 185–192, 2001.

[7] K. Kuhnen and P. Krejci, "Compensation of complex hysteresis and creep effects in piezoelectrically actuated systemsła new preisach modeling approach," *Automatic Control, IEEE Transactions on*, vol. 54, no. 3, pp. 537–550, 2009.

[8] A. Esbrook, X. Tan, and H. K. Khalil, "Control of systems with hysteresis via servocompensation and its application to nanopositioning," *Control Systems Technology, IEEE Transactions on*, vol. 21, no. 3, pp. 725–738, 2013.

[9] Y. Li and Q. Xu, "Adaptive sliding mode control with perturbation estimation and pid sliding surface for motion tracking of a piezo-driven micromanipulator," *Control Systems Technology, IEEE Transactions on*, vol. 18, no. 4, pp. 798–810, 2010.

[10] Z. Li, X. Zhang, G.-Y. Gu, X. Chen, and C.-Y. Su, "A comprehensive dynamic model for magnetostrictive actuators considering different input frequencies with mechanical loads," *IEEE Transactions on Industrial Informatics*, vol. 12, no. 3, pp. 980–990, 2016.

[11] M. Al Janaideh and D. S. Bernstein, "Adaptive control of hammerstein systems with unknown prandtl–ishlinskii hysteresis," *Proceedings of the Institution of Mechanical Engineers, Part I: Journal of Systems and Control Engineering*, vol. 229, no. 2, pp. 149–157, 2015.

[12] Z. Sun, L. Hao, B. Song, R. Yang, R. Cao, and Y. Cheng, "Periodic reference tracking control approach for smart material actuators with complex hysteretic characteristics," *Smart Materials and Structures*, vol. 25, no. 10, p. 105029, 2016.

[13] Z. Sun, B. Song, N. Xi, R. Yang, L. Hao, Y. Yang, and L. Chen, "Asymmetric hysteresis modeling and compensation approach for nanomanipulation system motion control considering working-range effect," *IEEE Transactions on Industrial Electronics*, 2017.

[14] M. Al Janaideh, S. Rakheja, and C.-Y. Su, "An analytical generalized prandtl–ishlinskii model inversion for hysteresis compensation in micropositioning control," *Mechatronics, IEEE/ASME Transactions on*, vol. 16, no. 4, pp. 734–744, 2011.

[15] I. D. Mayergoyz, *Mathematical models of hysteresis and their applications*. Academic Press, 2003.

[16] J. Zhang, E. Merced, N. Sepúlveda, and X. Tan, "Modeling and inverse compensation of nonmonotonic hysteresis in vo-coated microactuators," *Mechatronics, IEEE/ASME Transactions on*, vol. 19, no. 2, pp. 579–588, 2014.

[17] Z. Li, C.-Y. Su, and T. Chai, "Compensation of hysteresis nonlinearity in magnetostrictive actuators with inverse multiplicative structure for preisach model," *Automation Science and Engineering, IEEE Transactions on*, vol. 11, no. 2, pp. 613–619, 2014.

[18] M. Al Janaideh, M. Rakotondrabe, and O. Aljanaideh, "Further results on hysteresis compensation of smart micropositioning systems with the inverse prandtl–ishlinskii compensator," *IEEE Transactions on Control Systems Technology*, vol. 24, no. 2, pp. 428–439, 2016.

[19] G.-Y. Gu, C.-X. Li, L.-M. Zhu, and C.-Y. Su, "Modeling and identification of piezoelectric-actuated stages cascading hysteresis nonlinearity with linear dynamics," *IEEE/ASME Transactions on Mechatronics*, vol. 21, no. 3, pp. 1792–1797, 2016.

[20] K. Kuhnen, "Modeling, identification and compensation of complex hysteretic nonlinearities: A modified prandtl-ishlinskii approach," *European journal of control*, vol. 9, no. 4, pp. 407–418, 2003.

[21] Z. Sun, B. Song, N. Xi, R. Yang, L. Hao, and L. Chen, "Compensating asymmetric hysteresis for nanorobot motion control," in *Robotics and Automation (ICRA), 2015 IEEE International Conference on*. IEEE, 2015, pp. 3501–3506.

[22] R. Pintelon, P. Guillaume, Y. Rolain, J. Schoukens, and H. Van Hamme, "Parametric identification of transfer functions in the frequency domain-a survey," *Automatic Control, IEEE Transactions on*, vol. 39, no. 11, pp. 2245–2260, 1994.

[23] P. A. Parrilo, M. Sznaier, and R. S. S. Pena, "Mixed time/frequency-domain based robust identification," in *Decision and Control, 1996., Proceedings of the 35th IEEE Conference on*, vol. 4. IEEE, 1996, pp. 4196–4201.

[24] H. Lei, C. Lim, and X. Tan, "Modeling and inverse compensation of dynamics of base-excited ionic polymer–metal composite sensors," *Journal of Intelligent Material Systems and Structures*, p. 1045389X13478272, 2013.